

# Dynamical Simulations of Trapped Bose Gases at Finite Temperatures

B. Jackson and E. Zaremba

*Department of Physics, Queen's University, Kingston, Ontario K7L 3N6, Canada.*

(October 30, 2018)

## Abstract

In this paper, we develop a numerical procedure for investigating the dynamics of trapped Bose gases based on the ZGN theory. The dynamical equations used consist of a generalized Gross-Pitaevskii equation for the condensate order parameter and a semiclassical kinetic equation for the thermal cloud. The former is solved using a fast Fourier transform split-operator technique while the Boltzmann equation is treated by means of  $N$ -body simulations. The two components are coupled by mean fields as well as collisional processes that transfer atoms between the two. This scheme has been applied to a model equilibration problem, dipole oscillations in isotropic traps and scissors modes in anisotropic traps. In the case of the latter, the frequencies and damping rates of the condensate mode have been extracted from the simulations for a wide range of temperatures. Good agreement with recent experiments has been found.

PACS numbers: 03.75.Fi, 05.30.Jp, 67.40.Db

## I. INTRODUCTION

The achievement in 1995 of Bose-Einstein condensation (BEC) in trapped atomic gases [1–3] initiated a period of intense experimental and theoretical research which continues at an ever-increasing pace. Due to the relative diluteness of the atomic vapours, these systems present an excellent opportunity to investigate the effects of Bose degeneracy in novel situations. For example, a rich array of dynamical behaviour can occur as a result of the simultaneous occurrence of a condensate order parameter and thermal excitations.

It is now well established that at very low temperatures the dynamics of Bose-condensed gases can be accurately described by the Gross-Pitaevskii (GP) equation for the condensate order parameter (see e.g. [4]). However, despite considerable work over the past few years, it has proved far more difficult to extend the theory to include thermal excitations. One of the major challenges is to capture the dynamics of the non-condensed component in a self-consistent way, while still allowing for a feasible calculation. A possible approach to this problem was suggested by one of the authors (EZ) together with Griffin and Nikuni [5,6]. In this formalism (which we will hereafter denote by ZGN) the thermal excitations are described semiclassically by a Boltzmann kinetic equation, which couples to the condensate through mean fields and collisions.

In this paper we report on recent progress in solving the ZGN equations to study the dynamics of Bose-condensed gases in experimentally relevant regimes. We begin by briefly reviewing the formalism, and present analytical calculations of collision rates as a function of temperature. We then go on to discuss numerical calculations, where the kinetic equation is solved using  $N$ -body simulations with collisions treated through Monte-Carlo sampling. Applications to thermal cloud quenching, dipole modes, and scissors modes [7] are discussed. We conclude by highlighting future research directions.

## II. ZGN THEORY

The ZGN theory [6] is based on the assumption of a Bose broken symmetry which leads to the macroscopic wavefunction  $\Phi(\mathbf{r}, t) = \langle \hat{\psi}(\mathbf{r}, t) \rangle$ . Here,  $\hat{\psi}(\mathbf{r}, t)$  is the Bose field operator and the angular brackets denote an average with respect to a nonequilibrium density matrix. The condensate density is then given by  $n_c(\mathbf{r}, t) = |\Phi(\mathbf{r}, t)|^2$ . The condensate wavefunction is found to satisfy the generalized GP equation

$$i\hbar \frac{\partial}{\partial t} \Phi(\mathbf{r}, t) = \left( -\frac{\hbar^2}{2m} \nabla^2 + V(\mathbf{r}) + g[n_c(\mathbf{r}, t) + 2\tilde{n}(\mathbf{r}, t)] - iR(\mathbf{r}, t) \right) \Phi(\mathbf{r}, t), \quad (1)$$

where  $V(\mathbf{r})$  is the external confining potential,  $\tilde{n}(\mathbf{r}, t)$  is the noncondensate (or thermal atom) density, and  $R(\mathbf{r}, t)$  is a non-Hermitian source term that will be defined below. The interactions between atoms are taken to be local and leads to the mean field potential  $g[n_c + 2\tilde{n}]$ , where  $g = 4\pi\hbar^2 a/m$ , with  $a$  the  $s$ -wave scattering length. For  $T \rightarrow 0$ ,  $\tilde{n}$  and  $R$  are zero and one recovers the familiar nonlinear GP equation. The stationary ground state solution  $\Phi_0$  gives the density  $n_{c0} = |\Phi_0|^2$  which for large  $N$  is well-approximated by the Thomas-Fermi result  $n_{c0} = (\mu_0 - V)/g$  [4]. Here,  $\mu_0$  is the ground state GP eigenvalue or chemical potential.

Small amplitude excitations of the  $T = 0$  GP equation can be obtained by writing  $\Phi = \Phi_0 + \delta\Phi$  and linearizing with respect to the deviation  $\delta\Phi$ . This procedure is equivalent to the Hartree-Fock-Bogoliubov (HFB) approximation and generates the Bogoliubov quasiparticle excitations. At low energies, these excitations can be interpreted as collective excitations of the condensate, while at high energies they correspond to single-particle thermal excitations. However, at nonzero temperatures, one must take into account the occupation of excited states and the appearance of a noncondensate density  $\tilde{n}$  which interacts with the condensate. This problem was addressed by Hutchinson *et al.* [8] (hereafter referred to as HZG) and Dodd *et al.* [9] who calculated  $n_{c0}$  and  $\tilde{n}_0$  self-consistently in the HFB-Popov approximation. The quasiparticle excitations calculated within this scheme become temperature dependent and at first sight might be associated with collective excitations of the trapped gas. However these excitations in fact correspond to collective excitations of the condensate in the presence of a *static* thermal cloud. In other words, the dynamics of the latter are not included consistently. This was revealed in calculations of the center of mass dipole mode whose frequency showed a deviation from the trap frequency  $\omega_0$ , which is the correct result as dictated by the generalized Kohn theorem [10]. This was the motivation for developing a theory which consistently included the dynamics of the thermal cloud with that of the condensate.

The ZGN theory [6] provides such a description. It is based on the following approximations: (i) the Popov approximation which neglects the anomalous average  $\tilde{n}(\mathbf{r}, t) = \langle \tilde{\psi}(\mathbf{r}, t)\tilde{\psi}(\mathbf{r}, t) \rangle$ ; here,  $\tilde{\psi}(\mathbf{r}, t) \equiv \hat{\psi}(\mathbf{r}, t) - \langle \hat{\psi}(\mathbf{r}, t) \rangle$  is the noncondensate field operator, (ii) the use of Hartree-Fock thermal excitations with energy  $\varepsilon_{\mathbf{p}}(\mathbf{r}, t) = p^2/2m + U(\mathbf{r}, t)$ , where  $U = V + 2gn$  is the mean field potential acting on the thermal atoms, (iii) a semiclassical approximation for the thermal atoms which are represented by a phase-space distribution  $f(\mathbf{p}, \mathbf{r}, t)$ , and (iv) the inclusion of binary collisions among thermal atoms as well as with the condensate.

Within these approximations, one obtains the semiclassical Boltzmann kinetic equation for the thermal cloud

$$\frac{\partial f}{\partial t} + \frac{\mathbf{p}}{m} \cdot \nabla f - \nabla U \cdot \nabla_{\mathbf{p}} f = C_{12}[f] + C_{22}[f]. \quad (2)$$

The collision integrals appearing on the right hand side of this equation are given by

$$\begin{aligned} C_{12}[f] \equiv \frac{\sigma n_c}{\pi m^2} \int d\mathbf{p}_2 \int d\mathbf{p}_3 \int d\mathbf{p}_4 \delta(m\mathbf{v}_c + \mathbf{p}_2 - \mathbf{p}_3 - \mathbf{p}_4) \delta(\varepsilon_c + \varepsilon_2 - \varepsilon_3 - \varepsilon_4) \\ \times [\delta(\mathbf{p} - \mathbf{p}_2) - \delta(\mathbf{p} - \mathbf{p}_3) - \delta(\mathbf{p} - \mathbf{p}_4)] \\ \times [(1 + f_2)f_3f_4 - f_2(1 + f_3)(1 + f_4)], \end{aligned} \quad (3)$$

$$\begin{aligned} C_{22}[f] \equiv \frac{\sigma}{\pi h^3 m^2} \int d\mathbf{p}_2 \int d\mathbf{p}_3 \int d\mathbf{p}_4 \delta(\mathbf{p} + \mathbf{p}_2 - \mathbf{p}_3 - \mathbf{p}_4) \delta(\varepsilon + \varepsilon_2 - \varepsilon_3 - \varepsilon_4) \\ \times [(1 + f)(1 + f_2)f_3f_4 - f f_2(1 + f_3)(1 + f_4)]. \end{aligned} \quad (4)$$

Here,  $\sigma = 8\pi a^2$  is the total cross-section. The  $C_{22}$  integral involves the scattering of two atoms from initial to final thermal states. On the other hand,  $C_{12}$  describes collisions in which a condensate atom is involved in either the incoming or outgoing channels. These collisions have the effect of transferring atoms from or to the condensate and lead to a change in the number of noncondensate atoms,  $\tilde{N}$ . Specifically, we have

$$\frac{d\tilde{N}}{dt} = \int \frac{d\mathbf{r}d\mathbf{p}}{(2\pi\hbar)^3} C_{12}[f]. \quad (5)$$

These collisions also define the source term

$$R(\mathbf{r}, t) = \frac{\hbar}{2n_c} \int \frac{d\mathbf{p}}{(2\pi\hbar)^3} C_{12}[f] \quad (6)$$

appearing in Eq. (1). The condensate number  $N_c$  of course satisfies  $dN_c/dt = -d\tilde{N}/dt$  so that the total number of atoms,  $N = N_c + \tilde{N}$ , is conserved. The local rates at which atoms enter and leave the condensate are given by

$$\Gamma_{12}^{in} = \frac{\sigma n_c}{\pi h^3 m^2} \int d\mathbf{p}_2 \int d\mathbf{p}_3 \int d\mathbf{p}_4 \delta(m\mathbf{v}_c + \mathbf{p}_2 - \mathbf{p}_3 - \mathbf{p}_4) \delta(\varepsilon_c + \varepsilon_2 - \varepsilon_3 - \varepsilon_4) \times (1 + f_2) f_3 f_4. \quad (7)$$

$$\Gamma_{12}^{out} = \frac{\sigma n_c}{\pi h^3 m^2} \int d\mathbf{p}_2 \int d\mathbf{p}_3 \int d\mathbf{p}_4 \delta(m\mathbf{v}_c + \mathbf{p}_2 - \mathbf{p}_3 - \mathbf{p}_4) \delta(\varepsilon_c + \varepsilon_2 - \varepsilon_3 - \varepsilon_4) \times f_2 (1 + f_3) (1 + f_4). \quad (8)$$

In equilibrium,  $\mathbf{v}_c = 0$  and  $\varepsilon_c = \mu_0$ , the GP eigenvalue. One can then show that these two rates are equal if the distribution function takes its equilibrium Bose-Einstein form

$$f^0(\mathbf{p}, \mathbf{r}) = \frac{1}{\exp\{\beta(p^2/2m + U_0 - \mu_0)\} - 1}, \quad (9)$$

where  $\beta = 1/k_B T$ . As would be expected, the condensate and noncondensate must have the same chemical potential if the net transfer rate is to be zero. However, for the general nonequilibrium situation the  $\Gamma_{12}^{in(out)}$  rates are different and result in a time-dependent amplitude of the condensate wavefunction. This is revealed most clearly by making use of phase and amplitude variables,  $\Phi(\mathbf{r}, t) = \sqrt{n_c(\mathbf{r}, t)} e^{i\theta(\mathbf{r}, t)}$ . The generalized GP equation is then equivalent to the continuity equation

$$\frac{\partial n_c}{\partial t} + \nabla \cdot (n_c \mathbf{v}_c) = \Gamma_{12}^{in} - \Gamma_{12}^{out}, \quad (10)$$

where  $\mathbf{v}_c = \hbar \nabla \theta / m$ , and the Euler equation

$$m \frac{\partial \mathbf{v}_c}{\partial t} + \nabla \left( \frac{1}{2} m v_c^2 \right) = -\nabla \mu_c \quad (11)$$

with

$$\mu_c = -\frac{\hbar^2 \nabla^2 \sqrt{n_c}}{2m \sqrt{n_c}} + V + g n_c + 2g\tilde{n}. \quad (12)$$

It is instructive to examine  $\Gamma_{12}^{out}$  for an equilibrium state of a typical trapped gas.  $\Gamma_{12}^{out}$  represents the average number of thermal atoms colliding with the condensate per unit time per unit volume. Thus, dividing  $\Gamma_{12}^{out}$  by the local noncondensate density gives the

local equilibrium collision rate per atom,  $1/\tau_{12}^0$ , for this kind of collision [11]. In Fig. 1 we plot  $1/\tau_{12}^0$  for  $10^5$  Rb atoms in an isotropic trap with frequency  $\nu_0 = 200$  Hz for various temperatures below the ideal gas critical temperature  $T_c^0 \simeq 0.94\hbar\omega_0 N^{1/3}/k_B$ . The collision rate has a maximum at the edge of the condensate where the local fugacity  $z(r) = e^{\beta(\mu_0 - U_0)}$  approaches unity. Since  $1/\tau_{12}^0$  is proportional to  $n_{c0}$ , it falls off rapidly beyond this point. It is also interesting to note that for  $T$  approaching  $T_c^0$ ,  $\omega_0\tau_{12}^0 \leq 1$ , indicating that a thermal atom in this region of the condensate has a high probability of making a  $C_{12}$  collision on the timescale of the trap period. However, the number of thermal atoms which overlap with the condensate is relatively small and it is therefore more meaningful to define an average  $C_{12}$  collision rate per thermal atom by

$$\frac{1}{\bar{\tau}_{12}(T)} = \frac{1}{\tilde{N}(T)} \int d^3r \frac{\tilde{n}_0(r)}{\tau_{12}^0(r)}. \quad (13)$$

This quantity is plotted in Fig. 3 which shows that the thermal cloud is in the transition regime  $\omega_0\tau_{12}^0 \simeq 1$  rather than the truly hydrodynamic regime  $\omega_0\tau_{12}^0 \ll 1$  as the local collision rate in Fig. 1 suggests. Nevertheless, these results show that  $C_{12}$  collisions play an important role in the dynamics of the thermal cloud in the region of the condensate. Of course, the importance of these collisions increases with increasing  $N$  and one can expect to be in the hydrodynamic regime for  $N \geq 5 \times 10^5$  for this particular trap configuration.

One can also define an equilibrium collision rate between atoms in the thermal cloud. It is this rate that one would conventionally consider when deciding between collisionless and hydrodynamic behaviour. Accordingly, we define a  $C_{22}$  collision rate through the relation

$$\begin{aligned} \frac{\tilde{n}_0}{\tau_{22}^0} &\equiv \int \frac{d\mathbf{p}_1}{(2\pi\hbar)^3} C_{22}^{out}[f_1^0] \\ &= \frac{\sigma m^6}{4\pi\hbar^6} \int d\mathbf{v}_1 \int d\mathbf{v}_2 \int d\Omega v_r f_1^0 f_2^0 (1 + f_3^0)(1 + f_4^0). \end{aligned} \quad (14)$$

Here,  $C_{22}^{out}$  denotes the term in Eq. (4) in which particles in states ‘1’ and ‘2’ scatter into the final states ‘3’ and ‘4’. In equilibrium, the  $C_{22}^{out}$  and  $C_{22}^{in}$  terms are equal. In Eq. (14),  $\mathbf{v}_r = \mathbf{v}_1 - \mathbf{v}_2$  is the relative velocity of the incoming particles and the solid angle  $\Omega$  defines the orientation of the final relative velocity vector,  $\mathbf{v}'_r = \mathbf{v}_3 - \mathbf{v}_4$ . Momentum and energy conservation ensures that  $\mathbf{v}_1 + \mathbf{v}_2 = \mathbf{v}_3 + \mathbf{v}_4$  and  $v_r = v'_r$ . In the classical limit ( $\hbar \rightarrow 0$ ),  $1/\tau_{22}^0$  reduces to  $(1/\tau_{22}^0)_{cl} = \sqrt{2}\sigma v_{th}\tilde{n}_0$ , where  $v_{th} = (8kT/\pi m)^{1/2}$ . In Fig. 2 we plot  $1/\tau_{22}^0$  for the same trap parameters used to generate  $1/\tau_{12}^0$ . For  $T < T_c^0$ , we again see Bose enhancement of the  $C_{22}$  collision rate at the edge of the condensate, with  $\omega_0\tau_{22}^0 \ll 1$  being reached in this region at the higher temperatures. In Fig. 3 we present the average  $C_{22}$  collision rate  $1/\omega_0\bar{\tau}_{22}$ . Below  $T_c^0$ , this rate is comparable to the average  $C_{12}$  collision rate, indicating that the probability of a thermal atom colliding with another thermal atom is similar to the probability of colliding with the condensate. However, unlike  $1/\omega_0\bar{\tau}_{12}$  which involves the condensate density  $n_{c0}$ ,  $1/\omega_0\bar{\tau}_{22}$  continues to increase up to  $T_c^0$ , at which point it reaches a value of  $\omega_0\bar{\tau}_{22} \simeq 1$ . This limiting value increases with increasing  $N$ , indicating that the hydrodynamic regime is easily reached near  $T_c^0$ . Above  $T_c^0$ , the effect of Bose enhancement rapidly diminishes and the average rate approaches its classical limiting value.

### III. NUMERICAL METHODS

Eqs. (1) and (2) can in principle be used to describe the dynamics of a trapped Bose gas for arbitrary conditions of temperature, number of atoms and trap geometry. The equations have been solved previously for various limiting situations. For example, Eq. (1) was solved by HZG [8] for  $R = 0$  and with the assumption of a static thermal cloud. As stated earlier, this neglects the perturbation of the noncondensate that arises from the time-dependent mean-field of the oscillating condensate. As a result, it neglects those modes, such as the out-of-phase dipole mode, which involve the collective motion of the thermal atoms. Eqs. (1) and (2) have also been used to study collective modes in the collisionless limit using what is effectively a moment method [12]. In this approach, an ansatz for the form of the GP wavefunction and distribution function of the thermal cloud is made, and a finite number of moments of the GP and kinetic equations are retained to obtain a closed set of equations for the modes of interest. However, due to the truncation made, the effect of Landau damping on the modes is not included. Furthermore, the ansatz used for the form of the nonequilibrium distribution function does not treat the mean-field interactions between the two components accurately. In the opposite limit of high collision rates, we previously developed various approximations which address the dynamics in the hydrodynamic regime [6]. By assuming  $C_{22}$  collisions to be rapid we developed a description in which the thermal cloud is assumed to be in local thermodynamic equilibrium, but not necessarily in local equilibrium with the condensate [5]. The assumption of complete local equilibrium results in a Landau-Khalatnikov two-fluid theory [13,14].

Clearly it would be desirable to obtain accurate solutions of our equations which avoid approximations beyond those used to generate the equations themselves. In this way, the limitations of the approximations underlying the theory can be critically examined. For this purpose we have developed a numerical procedure within which the accuracy of the solutions can be studied and evaluated. We outline our numerical methods in the following.

The generalized GP equation can be solved by a split-operator technique. For the purposes of the following discussion, we write Eq. (1) in the operator form

$$i\hbar \frac{\partial \Phi}{\partial t} = (T + \tilde{V})\Phi, \quad (15)$$

where  $T$  is the kinetic energy operator and  $\tilde{V}$  is a complex, time-dependent potential. The wavefunction is advanced in time using the split-operator method:

$$\Phi(t + \Delta t) \simeq e^{-i\tilde{V}\Delta t/2\hbar} e^{-iT\Delta t/\hbar} e^{-i\tilde{V}\Delta t/2\hbar} \Phi(t). \quad (16)$$

Since the  $\tilde{V}$  operator is local in position space the effect of  $e^{-i\tilde{V}\Delta t/2\hbar}$  is most easily treated in the coordinate representation. The kinetic energy operator on the other hand is local in momentum space and it is therefore useful to Fourier transform the intermediate state when determining the effect of  $e^{-iT\Delta t/\hbar}$ . A fast fourier transform (FFT) routine is used for this purpose. The inverse transform is then applied in order to complete the evaluation of the evolution operator. Since  $\tilde{V}$  is time-dependent, a higher order approximant to the evolution operator is in fact used to increase the accuracy and stability of the GP equation solution.

The use of the semiclassical Boltzmann equation for the thermal atoms corresponds to a Hamiltonian description of the particle dynamics. In our case the Hamiltonian is simply

$H_{cl} = p^2/2m + U(\mathbf{r}, t)$ , where  $U(\mathbf{r}, t) = V(\mathbf{r}) + 2gn(\mathbf{r}, t)$  is the time-dependent mean-field potential. Thus the trajectory of a given atom between collisions can be determined using Newton's equations of motion. The evolution of the distribution function  $f(\mathbf{p}, \mathbf{r}, t)$  is then determined by considering the dynamics of  $N_T$  representative test particles [15–17] which in effect corresponds to the distribution function  $f_T(\mathbf{p}, \mathbf{r}, t) = \sum_{i=1}^{N_T} \delta(\mathbf{r} - \mathbf{r}_i)\delta(\mathbf{p} - \mathbf{p}_i)$ . In the absence of collisions, the dynamics of this swarm of test particles is equivalent to solving the collisionless Boltzmann equation.

In reality, the deterministic evolution of a particular phase space trajectory is interrupted stochastically by collisions with other atoms or with the condensate. In other words, in a time step  $\Delta t$ , a given thermal atom has some probability of suffering a collision, and the numerical algorithm used to generate these probabilities must yield collision rates that are consistent with the collision integrals in the Boltzmann equation. To simulate the  $C_{22}$  collisions [18], we bin the test particles into position space volume elements  $\Delta^3 r$ . Pairs of atoms ( $ij$ ) chosen at random from a given volume element define collision partners, and the probability of their suffering a collision in a time interval  $\Delta t$  is given by

$$P_{ij} = \tilde{n}\sigma|\mathbf{v}_i - \mathbf{v}_j| \int \frac{d\Omega}{4\pi} (1 + f_3)(1 + f_4)\Delta t. \quad (17)$$

The angular integral is an average over all possible orientations of the final relative velocity  $\mathbf{v}'_r$  and can be replaced by a single scattering event by choosing a random solid angle  $\Omega_R$  uniformly distributed on a unit sphere. Thus the probability used in the simulation is

$$P_{ij} = \tilde{n}\sigma|\mathbf{v}_i - \mathbf{v}_j|(1 + f_3^{\Omega_R})(1 + f_4^{\Omega_R})\Delta t. \quad (18)$$

The final velocities  $\mathbf{v}_3$  and  $\mathbf{v}_4$  are determined by  $\mathbf{v}_i$ ,  $\mathbf{v}_j$  and  $\Omega_R$  through momentum and energy conservation. To test whether a collision actually occurs, a random number  $R_{ij}$  distributed uniformly between 0 and 1 is chosen and compared to  $P_{ij}$ . If  $R_{ij}$  is less than  $P_{ij}$ , the collision is accepted. This process is repeated for each pair ( $ij$ ) in every real-space volume element. We have checked that the procedure correctly reproduces the equilibrium collision rates as given by Eq. (14).

The  $C_{12}$  collisions are treated in a similar fashion. In this case, both ‘in’ and ‘out’ collisions, as illustrated schematically in Fig. 4, must be considered separately since one of the incoming or outgoing particles is from the condensate. The overall rate of ‘out’ collisions is given by Eq. (8), in which a particle with velocity  $\mathbf{v}_2$  collides with the condensate to produce two outgoing thermal atoms with velocities  $\mathbf{v}_3$  and  $\mathbf{v}_4$ . This process is similar to a  $C_{22}$  collision in that the final relative velocity  $\mathbf{v}'_r = \mathbf{v}_3 - \mathbf{v}_4$  can have arbitrary direction with a magnitude of  $v'_r = \sqrt{|\mathbf{v}_c - \mathbf{v}_2|^2 - 4gn_c/m}$ . This value is a consequence of energy conservation and accounts for the fact that the mean-field energy of a thermal atom differs from that of a condensate atom by  $gn_c$ . Choosing one of the test particles,  $i$ , from the volume element  $\Delta^3 r$ , the probability of it suffering an ‘out’ collision is given by

$$P_i^{out} = n_c\sigma v'_r(1 + f_3^{\Omega_R})(1 + f_4^{\Omega_R})\Delta t. \quad (19)$$

The situation for ‘in’ collisions is somewhat more complex since an arbitrary pair of thermal atoms in  $\Delta^3 r$  will be precluded by energy and momentum conservation from scattering into the condensate. To ensure that these collision events are sampled correctly, we rewrite

Eq. (7) by interchanging the ‘2’ and ‘3’ labels in the integral. The ‘2’-particle is then paired with the ‘4’-particle to produce the outgoing ‘3’-particle. The resulting integral leads to a significantly different form for the probability of this type of collision event. Without giving details, we find that ( $i = \text{‘2’}$ )

$$P_i^{in} = \frac{n_c \sigma \mathcal{A}_v}{\pi |\mathbf{v}_i - \mathbf{v}_c|} (1 + f_3^{\mathbf{v}_R}) f_4^{\mathbf{v}_R} \Delta t, \quad (20)$$

where  $\mathbf{v}_R$  is a random point in a plane of area  $\mathcal{A}_v$  in velocity space. The plane is defined by energy and momentum conservation, and once the velocity  $\mathbf{v}_R$  is chosen, the velocities  $\mathbf{v}_3$  and  $\mathbf{v}_4$  are determined.  $P_i^{in}$  is largely independent of  $\mathcal{A}_v$  as long as the plane completely samples the occupied regions of phase space. We have checked that  $P_i^{out}$  and  $P_i^{in}$  give identical collision rates for the equilibrium situation. The simulation of  $C_{12}$  collisions then proceeds as follows. For each particle  $i$  in  $\Delta^3 r$ ,  $P_i^{out}$  and  $P_i^{in}$  are calculated. A random number  $R_i$  is selected and if  $R_i > P_i^{in} + P_i^{out}$ , no collision occurs, while if  $R_i < P_i^{in}$ , the ‘in’ collision is accepted and if  $P_i^{in} < R_i < P_i^{in} + P_i^{out}$ , the ‘out’ collision is accepted. This procedure ensures that any given particle only makes one kind of collision, if a collision occurs at all. We have again checked that this prescription gives correctly the equilibrium ‘in’ and ‘out’ collision rates.

We finally address the question of determining the mean-field potential,  $2g\tilde{n}$ , for  $N_T$  point-like test particles. An approximation to  $\tilde{n}(\mathbf{r})$  is obtained by dividing space into cells  $\Delta^3 r$  and binning the distribution to construct a density histogram. If  $\Delta^3 r$  is sufficiently small and  $N_T$  sufficiently large, this procedure will generate a fairly smooth density distribution. Since our simulations are restricted practically to  $N_T < 10^6$  and a three-dimensional spatial grid that is relatively coarse, statistical fluctuations in the number histogram are inevitable. To compensate for these fluctuations we have adopted the following strategy. First, we use a cloud-in-cell method [19] to define density weights at the 8 grid points bounding a cell according to the position of a particle within the cell. Having defined a density on the grid points of our mesh, we next convolve the density with a gaussian:

$$\tilde{n}_{conv}(\mathbf{r}) = \frac{1}{\pi^{3/2} \eta^3} \int d\mathbf{r}' e^{-|\mathbf{r}-\mathbf{r}'|^2/\eta^2} \tilde{n}(\mathbf{r}'). \quad (21)$$

By choosing a width parameter  $\eta$  somewhat larger than the spatial grid used in our calculations, we achieve a further smoothening of the thermal atom density. The final mean-field potential of the thermal atoms is then defined as  $2g\tilde{n}_{conv}(\mathbf{r})$ . This result can also be viewed in terms of an interaction potential  $g(\mathbf{r} - \mathbf{r}') = (g/\pi^{3/2}\eta^3) \exp(-|\mathbf{r} - \mathbf{r}'|^2/\eta^2)$  which has a finite range  $\eta$  as opposed to the contact interaction  $g\delta(\mathbf{r} - \mathbf{r}')$  usually assumed. Such a procedure has a minor effect for density variations on length scales larger than  $\eta$  but has the benefit of reducing fluctuations stochastically generated on the scale of the spatial grid. We can of course check that the physical properties of interest are unaffected by the value of  $\eta$  used in the calculations. The gaussian convolution has the further useful feature of being readily calculable with a FFT routine.

Our simulations commence with the specification of the initial state of the system, namely the condensate wavefunction  $\Phi(\mathbf{r}, 0)$  and the initial distribution of test particles. The particular choice is dictated by the physical situation being treated and several examples are considered in the following section. Once the initial state is known, the condensate and

noncondensate mean-field potentials are determined. The condensate wavefunction is propagated for a time  $\Delta t$  and the test particle positions and momenta are updated. At the end of this time step, the  $C_{22}$  and  $C_{12}$  collisions are considered in turn and their net effect on the thermal cloud distribution is determined. At the same time, the  $C_{12}$  collisions are accumulated to construct the source term  $R(\mathbf{r}, t)$  that is needed for the next cycle in the GP evolution. This procedure is then repeated for the duration of the simulation. Quantities of physical interest can be calculated from the condensate wavefunction and test particle distribution at each time step and are recorded for subsequent analysis and display.

## IV. APPLICATIONS

### A. Equilibration

We begin by considering a relatively simple model problem which illustrates the equilibration of an initial nonequilibrium state. We imagine a trapped gas in equilibrium at some temperature  $T_0$  which is chosen such that approximately half of the atoms are in the condensate. To be specific, we consider  $5 \times 10^4$   $^{87}\text{Rb}$  atoms in an isotropic trap with harmonic frequency  $\nu_0 = 187$  Hz. The scattering length is  $a = 5.82$  nm. The equilibrium state is determined by solving self-consistently the following pair of equations:

$$-\frac{\hbar^2 \nabla^2}{2m} \Phi_0(\mathbf{r}) + [V(\mathbf{r}) + gn_{c0}(\mathbf{r}) + 2g\tilde{n}_0(\mathbf{r})] \Phi_0(\mathbf{r}) = \mu_0 \Phi_0(\mathbf{r}), \quad (22)$$

and

$$\tilde{n}_0(\mathbf{r}) = \frac{1}{\Lambda^3} g_{3/2}(z_0(\mathbf{r})), \quad (23)$$

where  $\Lambda = (2\pi\hbar^2/mkT_0)^{1/2}$  is the thermal de Broglie wavelength,  $z_0(\mathbf{r}) = \exp(\beta_0(\mu_0 - U_0(\mathbf{r})))$  is the local equilibrium fugacity,  $\beta_0 = 1/k_B T_0$  and  $U_0(\mathbf{r}) = V(\mathbf{r}) + 2g[n_{c0}(\mathbf{r}) + \tilde{n}_0(\mathbf{r})]$ . For  $T_0 = 200$  nK, we find  $N_{c0} = 2.58 \times 10^4$ . We next define a nonequilibrium state by first constructing a sample of test particles representative of the equilibrium density  $\tilde{n}_0(r)$ . Each of these particles is then distributed in momentum according to the phase space distribution  $f(\mathbf{p}, \mathbf{r}) = (\Lambda/\Lambda_0)^3 [z_0(\mathbf{r})^{-1} \exp(\beta p^2/2m) - 1]^{-1}$ , where the temperature  $T$  is half the equilibrium value  $T_0$ . This initial nonequilibrium state has a total density equal to the equilibrium distribution, but the cloud is too ‘cold’ to sustain this distribution as a function of time. It begins to collapse in real space, with  $C_{12}$  collisions simultaneously transferring atoms from the thermal cloud to the condensate. In Fig. 5 we show the evolution of the condensate and noncondensate numbers as a function of time. One can see that the condensate number relaxes to a higher value corresponding to a final equilibrium temperature  $T' < T_0$ , on a timescale expected on the basis of the equilibrium  $C_{12}$  collision rates. The figure also shows the total number of atoms,  $N = N_C + \tilde{N}$ , as a function of time in the simulation. This number should of course be constant but the simulation does not conserve particle number exactly at each time step because of the different ways in which particle number is changed in the condensate and thermal cloud. The Monte-Carlo sampling of collisions leads to integer-valued changes in the number of thermal test particles. On the other hand, the normalization of the condensate changes quascontinuously at a rate determined by the

strength of the source term  $R(\mathbf{r}, t)$  in the GP equation. The fact that  $N$  in our simulations exhibits only small fluctuations about the initial value is reassuring and demonstrates that number conservation is preserved in an average sense. This is an obvious requirement of any method that hopes to address problems such as condensate growth [20].

In Fig. 6 we show the root-mean-squared radius  $\sqrt{\langle r^2 \rangle}$  of both the condensate and thermal cloud. The thermal cloud initially begins to collapse as a result of the quench before bouncing back and oscillating at a frequency very close to the monopole frequency  $2\omega_0$  of a noninteracting thermal cloud. Oscillations in the condensate are in turn induced by the time-dependent mean-field potential as well as by the condensation of thermal atoms. These oscillations at first build up in time and then damp out as the entire system approaches overall equilibrium. The frequency of these oscillations is about 5% lower than the TF frequency for the condensate monopole mode,  $\sqrt{5}\omega_0$  [21]. This confirms that our simulations are providing a good description of the dynamical behaviour of both the condensate and thermal cloud.

## B. Dipole Oscillations

Our second example is perhaps an even more stringent test of our numerical procedures. For harmonic confinement, a trapped gas must exhibit a centre of mass oscillation in which the total density of the gas oscillates rigidly without change in shape at the trap frequency  $\omega_0$ , i.e.,  $n(\mathbf{r}, t) = n_0(\mathbf{r} - \boldsymbol{\eta}(t))$ , with  $\boldsymbol{\eta}(t) = \boldsymbol{\eta}_0 \cos(\omega_0 t)$ . This result is a consequence of the generalized Kohn theorem [10] and must be satisfied in any consistent theory of the dynamics. The failure to satisfy this property was the signature that the HFBP mode calculations were deficient [8]. The ZGN theory, however, is formally consistent with the generalized Kohn theorem [6]. Our purpose here is to demonstrate that our numerical implementation of the theory satisfies this requirement as well.

In these simulations, we retain the same trap parameters as given in the previous subsection and the same number of Rb atoms, but at a higher temperature ( $T_0 = 225$  nK) where the difference between the condensate and noncondensate numbers is larger. The reason for wanting this difference to be appreciable will become apparent shortly. We begin by obtaining the equilibrium condensate wavefunction and an equilibrium distribution of test particles. To excite the dipole oscillations, we then displace each component a small distance  $\Delta z$  along the  $z$ -axis relative to the trap, but in opposite directions. This is easily achieved by shifting the condensate wavefunction a certain number of grid points on the spatial mesh, and adding a constant displacement  $\Delta z$  to the position of each test particle. The two components are then released and their subsequent motion is determined.

In our first simulation, we turn off all collisional processes. The two components then interact only as a result of the mean-field potentials. The mean displacement of the condensate,  $\langle z_c(t) \rangle = \int d\mathbf{r} z n_c(\mathbf{r}, t) / N_c$ , and the thermal cloud,  $\langle \tilde{z}(t) \rangle = \sum_{i=1}^{N_T} z_i(t) / N_T$ , are then calculated as a function of time. In Fig. 7 we plot the center of mass position

$$Z_{cm}(t) = \frac{1}{N} \left( N_c \langle z_c(t) \rangle + \tilde{N} \langle \tilde{z}(t) \rangle \right), \quad (24)$$

and the relative displacement

$$z(t) = \langle z_c(t) \rangle - \langle \tilde{z}(t) \rangle. \quad (25)$$

We see that  $Z_{cm}(t)$  oscillates at the trap frequency,  $\omega_0$ , as expected, with no change in amplitude. This amplitude is given by  $Z_{cm}(0) = \Delta z(\tilde{N} - N_c)/N$  and is non-zero because  $\tilde{N} \neq N_c$  in the equilibrium state. The relative displacement  $z(t)$  is also shown, and it is seen to decay as a function of time, although its behaviour at longer times is more complex.

These results can be interpreted in terms of a two mode model [6]: (i) a centre-of-mass mode for which  $\langle z_c(t) \rangle_1 / \langle \tilde{z}(t) \rangle_1 = 1$  and (ii) an out-of-phase dipole mode for which  $\langle z_c(t) \rangle_2 / \langle \tilde{z}(t) \rangle_2 = -\tilde{N}/N_c$ . Within this picture, the initial displacement of the two components excites a superposition of these two modes and the individual displacements are given by

$$\begin{aligned} \langle z_c(t) \rangle &= \left[ \left( (\tilde{N} - N_c)/N \right) \cos \omega_1 t - (2\tilde{N}/N) \cos \omega_2 t \right] \Delta z, \\ \langle \tilde{z}(t) \rangle &= \left[ \left( (\tilde{N} - N_c)/N \right) \cos \omega_1 t + (2N_c/N) \cos \omega_2 t \right] \Delta z, \end{aligned} \quad (26)$$

where  $\omega_1$  and  $\omega_2$  are the two mode frequencies. In this model,  $Z_{cm}(t) = \Delta z(\tilde{N} - N_c)/N \cos \omega_1 t$  and  $z(t) = -\Delta z(4\tilde{N}/N) \cos \omega_2 t$ . These expressions qualitatively describe the results of the full simulation, although the relative displacement is actually damped as a result of coupling to other internal degrees of freedom. As the condensate moves through the thermal cloud, the thermal atoms experience a time-dependent mean-field potential which can transfer energy to them. This excitation mechanism is the source of Landau damping of the mode. However, the interplay between the internal degrees of freedom and the out-of-phase collective variable is complex and is the reason why  $z(t)$  does not exhibit a simple damped-exponential behaviour.

In our second dipole simulation, we include both the  $C_{12}$  and  $C_{22}$  collision processes. The qualitative behaviour is similar to our previous simulation in that the centre-of-mass mode continues to oscillate without damping at the trap frequency,  $\omega_0$ . This is the signature that the generalized Kohn theorem is being satisfied. In contrast to the centre-of-mass mode, the out-of-phase dipole mode is damped. Interestingly, the behaviour is more regular than in the absence of collisions. The damping is still due to the Landau mechanism, but as these mean-field excitations proceed, collisions are continually driving the gas towards local equilibrium. These collisions limit the extent to which the thermal cloud phase space distribution can be driven out of equilibrium, and as a result, the complex long-time behaviour seen in the absence of collisions is eliminated.

### C. Scissors Mode Oscillations

As our final application, we consider the scissors mode oscillations that have recently been studied in anisotropic traps [22,23]. A preliminary report of our work has appeared [7] and we shall here summarize some of the main findings.

We consider an anisotropic harmonic trap of the form  $V(\mathbf{r}) = m(\omega_\rho^2 \rho^2 + \omega_z^2 z^2)/2$  which has axial symmetry about the  $z$ -axis, with  $\omega_z \simeq \sqrt{8}\omega_\rho$ . In the experiments [23], the scissors mode is excited by adiabatically rotating the trap potential through a small angle  $\theta_0$  and then suddenly rotating the trap through an angle  $-2\theta_0$ . To simulate this process, we first determine the equilibrium state of the system at some temperature  $T$  using the method outlined earlier. We then rotate the particle coordinates and condensate wavefunction relative

to the trapping potential through an angle  $2\theta_0$  about the  $y$ -axis. At this point the dynamical simulations commence.

The relevant dynamical variables in this situation are the  $xz$ -quadrupole moments  $Q_c(t) = \int d\mathbf{r} xz n_c(\mathbf{r}, t)$  and  $\tilde{Q}(t) = (\tilde{N}/N_T) \sum_{i=1}^{N_T} x_i(t) z_i(t)$ . If we assume that the two components rotate about the  $y$ -axis without distortion, these quadrupole moments would be given by  $Q_\alpha = \theta(t) Q_\alpha^0$ , where  $\theta(t)$  is the instantaneous rotation angle and  $Q_\alpha^0 = \langle x^2 - z^2 \rangle_\alpha^0$  is the equilibrium quadrupole moment of the  $\alpha$ -th component. We thus define the ‘rotation angle’  $\theta_\alpha(t) \equiv Q_\alpha(t)/Q_\alpha^0$  as the variable representing the angular displacement of the two components in our simulations. The advantage of using the angular variables is that the range of angular displacements is similar for both components, and independent of temperature, in contrast to the quadrupole moments.

In Figs. 8-10 we show the angular displacements of the two components as a function of time for a few temperatures. At the intermediate temperature of  $T = 185$  nK,  $N_c/N = 0.33$ , and we see the condensate exhibiting a damped oscillation at a single frequency, while the thermal cloud oscillation consists of a superposition of two frequencies. This is to be expected on the basis of the modes that are found at low temperatures for a pure condensate and for a thermal cloud above  $T_c^0$  [24]. For the  $T = 0$  condensate, a straightforward analysis of the linearized TF equations of motion which follow from Eqs. (10)-(12) allows one to determine the scissors mode frequency. Multiplying the continuity equation by  $xz$  and integrating over all space leads to

$$\frac{d}{dt} \langle xz \rangle = \langle xv_{cz} + zv_{cx} \rangle, \quad (27)$$

where the velocity moments are defined as  $\langle x_i v_{cj} \rangle = \int d\mathbf{r} x_i v_{cj}(\mathbf{r}, t) n_{c0}(\mathbf{r})$ . Taking these moments of the velocity equation gives

$$\frac{d}{dt} \langle xv_{cz} + zv_{cx} \rangle = -(\omega_x^2 + \omega_z^2) \langle xz \rangle. \quad (28)$$

These equations define the condensate scissors mode with frequency  $\omega_{sc} = \sqrt{\omega_x^2 + \omega_z^2}$ . Our  $T = 0$  simulations for  $N = 2 \times 10^4$  yield a frequency which is 1.5% larger than the TF result due to finite number effects.

A similar moment analysis can be carried out for the Boltzmann equation above  $T_c^0$  [24]. One obtains the following moment equations

$$\begin{aligned} \frac{d}{dt} \langle xz \rangle &= \langle xv_z + zv_x \rangle \\ \frac{d}{dt} \langle xv_z - zv_x \rangle &= 2\epsilon\omega_0^2 \langle xz \rangle \\ \frac{d}{dt} \langle xv_z + zv_x \rangle &= 2\langle v_x v_z \rangle - 2\omega_0^2 \langle xz \rangle \\ \frac{d}{dt} \langle v_x v_z \rangle &= -\omega_0^2 \langle xv_z + zv_x \rangle - \epsilon\omega_0^2 \langle xv_z - zv_x \rangle - \frac{\langle v_x v_z \rangle}{\tau}, \end{aligned} \quad (29)$$

where  $\epsilon = (\omega_z^2 - \omega_x^2)/(\omega_z^2 + \omega_x^2)$  and  $\omega_0^2 = (\omega_x^2 + \omega_z^2)/2$ . In the collisionless limit ( $\tau \rightarrow \infty$ ), these equations yield two scissors modes with frequencies  $\omega_\pm = \omega_z \pm \omega_\rho$ . Our simulations above  $T_c^0$  agree well with these predictions. As Figs. 8-10 indicate, these modes persist down to

quite low temperatures below  $T_c^0$  due to the relatively weak mean-field interactions between the condensate and thermal cloud.

We now discuss the temperature dependence of the scissors mode oscillations. Fig. 8 shows results for  $T = 55$  nK and  $N_c/N = 0.95$ . The condensate mode is only weakly damped with a frequency which is close to the  $T = 0$  limit. However, the dynamics of the thermal cloud is quite different from the behaviour seen at higher temperatures. At this low temperature, the dynamics of the thermal cloud is strongly affected by the condensate mean-field. The fact that the thermal cloud shows an oscillation at the condensate frequency is indicative of its being driven by the more massive condensate. With increasing temperature, this coupling weakens and the thermal cloud begins to display its own scissors mode frequencies (Fig. 9). At the same time, the damping of the condensate mode is seen to increase as a result of the increasing rate of Landau damping. Finally, at the highest temperature of 296 nK shown in Fig. 10,  $N_c/N = 0.02$ , and the roles of condensate and thermal cloud are reversed in that the condensate is strongly coupled to the more massive thermal cloud and exhibits a more complex oscillation pattern.

The interaction between the condensate and thermal cloud in the course of their oscillations is revealed by a density contour plot for the two components. This is shown in Fig. 11 for a sequence of equally spaced time steps spanning approximately half a period of the condensate oscillation. What is striking about this figure is the lack of any obvious distortion of the condensate. It appears very much to be a rigid body (but not in a rotational sense!) as it oscillates in the anisotropic trap. The thermal component on the other hand shows clear signs of its interaction with the repulsive mean-field of the condensate. The condensate tends to move the thermal cloud out of its way in the course of its motion, much like a boat moving through water. Clearly the thermal cloud is strongly perturbed in the vicinity of the condensate. It is here that excitation of the thermal atoms, which leads to Landau damping of the condensate oscillation, occurs most strongly.

A comparison of our results with experiment is shown in Fig. 12. To obtain the frequencies and damping rates of the various scissors modes we make the assumption that the calculated time-dependent quadrupole moments are a superposition of three normal modes, one corresponding to the condensate scissors mode and the other two to the thermal cloud scissors modes. Accordingly, we fit the time-dependent data in Figs. 8-10 with three damped sinusoidal functions with adjustable amplitudes. The values of the frequency and damping rate of the condensate scissors mode extracted in this way are found to be in very good agreement with experiment for  $T < 0.8T_c^0$ . Discrepancies occur above this temperature, but here the experimental error bars are quite large. As discussed above, the condensate is strongly coupled to the thermal cloud as  $T_c^0$  is approached and it becomes difficult to obtain good fits to the condensate quadrupole moment using the three-mode analysis. This is probably also the source of the large error bars associated with the experimental fits.

At low temperatures, the frequency of the condensate mode at first increases slightly with increasing temperature. This we believe is due to an increasing deviation from the TF frequency  $\sqrt{\omega_\rho^2 + \omega_z^2}$  as a result of the decreasing number of condensate atoms. At higher temperatures, the frequency begins to decrease as a result of the increasing size of the thermal cloud. As the density contours in Fig. 11 suggest, the condensate drags part of the thermal cloud along with it and one would expect the condensate to effectively have a larger inertia, and therefore a lower frequency. The damping of the condensate mode is essentially

due to Landau damping but  $C_{12}$  and  $C_{22}$  collisions are indirectly playing an important role. Without collisions, the damping rate is as much as 50% lower than the values shown in the figure. Collisions have the effect of equilibrating the thermal cloud which is being driven by the condensate, and it appears that this internal equilibration is enhancing the rate at which excitations of thermal atoms occur.

The existence of a single condensate scissors mode is a consequence of the irrotational nature of the condensate velocity field. In contrast, the velocity fields of each of the two thermal cloud modes have both irrotational and solenoidal components. This distinction becomes apparent in the moment of inertia of the system,  $I$ . Zambelli and Stringari [25] have shown that the moment of inertia is given by the expression

$$\frac{I}{I_{\text{rigid}}} = (\omega_z^2 - \omega_\rho^2)^2 \frac{\int d\omega \chi''(\omega)/\omega^3}{\int d\omega \chi''(\omega) \omega}, \quad (30)$$

where  $I_{\text{rigid}}$  is the moment inertia of the system treated as a rigid body. The quantity  $\chi''(\omega)$  is the imaginary part of the quadrupole response function of the system:

$$\chi(\omega) = \frac{i}{\hbar} \int_0^\infty dt \langle [\hat{Q}(t), \hat{Q}(0)] \rangle_0, \quad (31)$$

where  $\hat{Q} = \sum_{i=1}^N \hat{x}_i \hat{z}_i$  is the quadrupole moment operator. This function determines the linear response of the system to an arbitrary time-dependent perturbation that couples to  $\hat{Q}$ . In particular, the sudden rotation of the trap through a small angle  $\theta_0$  induces the time-dependent quadrupole moment  $Q(t)$  determined in our simulations. It can be shown that

$$\chi''(\omega) = -\omega \Re \left\{ \tilde{Q}'(\omega)/\lambda \right\}, \quad (32)$$

where  $\tilde{Q}'(\omega)$  is the Fourier transform of  $Q(t) - Q(\infty)$  and  $\lambda = m(\omega_z^2 - \omega_x^2)\theta_0$ . Our three-mode analysis of the induced quadrupole moment yields a  $\chi''(\omega)$  consisting of a sum of Lorentzian spectral densities for which the frequency moments required in Eq. (30) are undefined. However, the moment of inertia can be estimated by replacing the Lorentzian line shapes by delta functions having the same spectral weight. Using this procedure, we show the moment of inertia of the system as a function of temperature in Fig. 13. At high temperatures,  $I$  tends towards  $I_{\text{rigid}} = m\langle x^2 + z^2 \rangle N$ , as expected when the large thermal cloud dominates the response. On the other hand, as  $T \rightarrow 0$ , the moment of inertia takes on the irrotational value,  $I = \bar{\epsilon}^2 I_{\text{rigid}}$ , where  $\bar{\epsilon} = \langle x^2 - z^2 \rangle_c^0 / \langle x^2 + z^2 \rangle_c^0$  parameterises the deformation of the condensate in equilibrium.

Under the semiclassical approximation, Stringari [26] showed (at least in the ideal gas case) that  $I$  at intermediate temperatures is simply the sum of the two limiting values, weighted by the number of atoms in each component

$$I = \bar{\epsilon}^2 m \langle x^2 + z^2 \rangle_c N_c + m \langle x^2 + z^2 \rangle_n \tilde{N}. \quad (33)$$

This quantity can be readily calculated from the equilibrium densities and is plotted (as a ratio with  $I_{\text{rigid}}$ ) in Fig. 13. Comparison to the results from (30) show that both monotonically increase with rising temperature, clearly indicating the transition between superfluid and normal fluid behaviour. Small discrepancies between the two approaches may result from our evaluation of the frequency spectrum, or in generalising (33) to an interacting gas.

## V. CONCLUSIONS

We have used the ZGN theory to investigate the dynamics of trapped Bose gases at finite temperatures. In this theory, the condensate is described by a generalized GP equation while the thermal cloud is treated semiclassically in terms of a Boltzmann kinetic equation. We have developed a numerical procedure for solving these equations and have applied the method to a variety of dynamical problems including equilibration and collective excitations. We have demonstrated that the ZGN theory provides an effective method for dealing with such problems and is a useful tool in the interpretation of experiment. In particular, the method has been used to examine the scissors modes in anisotropic traps. The good agreement with experiment found for this entire class of modes is encouraging and suggests that other situations can also be analyzed successfully. We plan to continue this work with a systematic study of the various collective modes that have been probed experimentally, as well as problems associated with vortex nucleation and dynamics.

## ACKNOWLEDGMENTS

We acknowledge financial support from the Natural Sciences and Engineering Research Council of Canada, and the use of the HPCVL computing facilities at Queen's. We thank A. Griffin, J. Williams and T. Nikuni for valuable discussions.

## REFERENCES

- [1] M. H. Anderson, J. R. Ensher, M. R. Matthews, C. E. Wieman, and E. A. Cornell, *Science* **269**, 198 (1995).
- [2] C. C. Bradley, C. A. Sackett, J. J. Tollett, and R. G. Hulet, *Phys. Rev. Lett.* **75**, 1687 (1995).
- [3] K. B. Davis, M. O. Mewes, M. R. Andrews, N. J. van Druten, D. S. Durfee, D. M. Kurn, and W. Ketterle, *Phys. Rev. Lett.* **75**, 3969 (1995).
- [4] F. Dalfovo, S. Giorgini, L. P. Pitaevskii, and S. Stringari, *Rev. Mod. Phys.* **71**, 463 (1999).
- [5] T. Nikuni, E. Zaremba, and A. Griffin, *Phys. Rev. Lett.* **83**, 10 (1999).
- [6] E. Zaremba, T. Nikuni, and A. Griffin, *J. Low Temp. Phys.* **116**, 277 (1999).
- [7] B. Jackson and E. Zaremba, e-print cond-mat/0105465.
- [8] D. A. W. Hutchinson, E. Zaremba, and A. Griffin, *Phys. Rev. Lett.* **78**, 1842 (1997).
- [9] R. J. Dodd, M. Edwards, C. W. Clark, and K. Burnett, *Phys. Rev. A* **57**, R32 (1998).
- [10] J. F. Dobson, *Phys. Rev. Lett.* **73**, 7244 (1994), and references therein.
- [11] We note that  $\tau_{12}^0$  is defined differently in Ref. [5]. There, the  $\Gamma_{12}^{out}$  collision rate is divided by  $n_{c0}$ , rather than by  $\tilde{n}_0$  as done here. The latter is a more useful definition for the purpose of comparing  $C_{12}$  and  $C_{22}$  collision rates.
- [12] M. Bijlsma and H. T. C. Stoof, *Phys. Rev. A* **60**, 3973 (1999).
- [13] I. K. Khalatnikov, *An Introduction to the Theory of Superfluidity*, W. A. Benjamin, New York (1965).
- [14] T. Nikuni and A. Griffin, *Phys. Rev. A* **63**, 033608 (2001).
- [15] G. A. Bird, *Molecular Gas Dynamics and the Direct Simulation of Gas Flows* (Oxford University Press, Oxford, 1994).
- [16] H. Wu, E. Arimondo, and C. J. Foot, *Phys. Rev. A* **56**, 560 (1997).
- [17] T. Lopez-Arias and A. Smerzi, *Phys. Rev. A* **58**, 526 (1998).
- [18] B. Jackson and C. S. Adams, *Phys. Rev. A* **63**, 053606 (2001).
- [19] R. W. Hockney and J. W. Eastwood, *Computer simulations using particles* (McGraw-Hill, New York, 1981).
- [20] M. Bijlsma, E. Zaremba and H. T. C. Stoof, *Phys. Rev. A* **62**, 063609 (2000).
- [21] S. Stringari, *Phys. Rev. Lett.* **77**, 2360 (1996).
- [22] O. M. Maragò, S. A. Hopkins, J. Arlt, E. Hodby, G. Hechenblaikner, and C. J. Foot, *Phys. Rev. Lett.* **84**, 2056 (2000).
- [23] O. M. Maragò, G. Hechenblaikner, E. Hodby, and C. J. Foot, *Phys. Rev. Lett.* **86**, 3938 (2001).
- [24] D. Guery-Odelin and S. Stringari, *Phys. Rev. Lett.* **83**, 4452 (1999).
- [25] F. Zambelli and S. Stringari, *Phys. Rev. A* **63**, 033602 (2001).
- [26] S. Stringari, *Phys. Rev. Lett.* **76**, 1405 (1996).

FIGURES

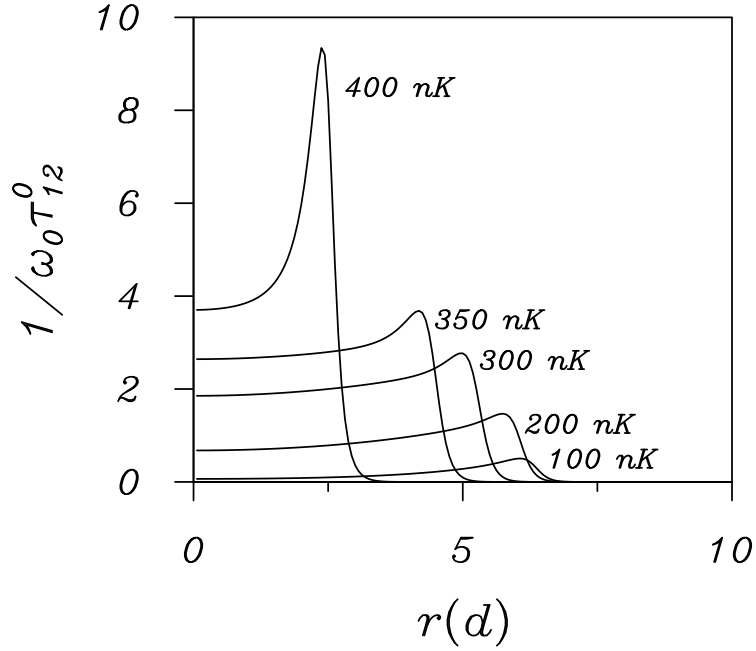


FIG. 1. The equilibrium local  $C_{12}$  collision rate  $1/\tau_{12}^0$  in units of the trap frequency,  $\omega_0$ , as a function of the radial distance in units of the harmonic oscillator length  $d = \sqrt{\hbar/m\omega_0}$ . The different curves are labelled by the temperature  $T$ . The trap is isotropic with harmonic frequency  $\nu_0 = 200$  Hz and contains  $10^5$   $^{87}\text{Rb}$  atoms.

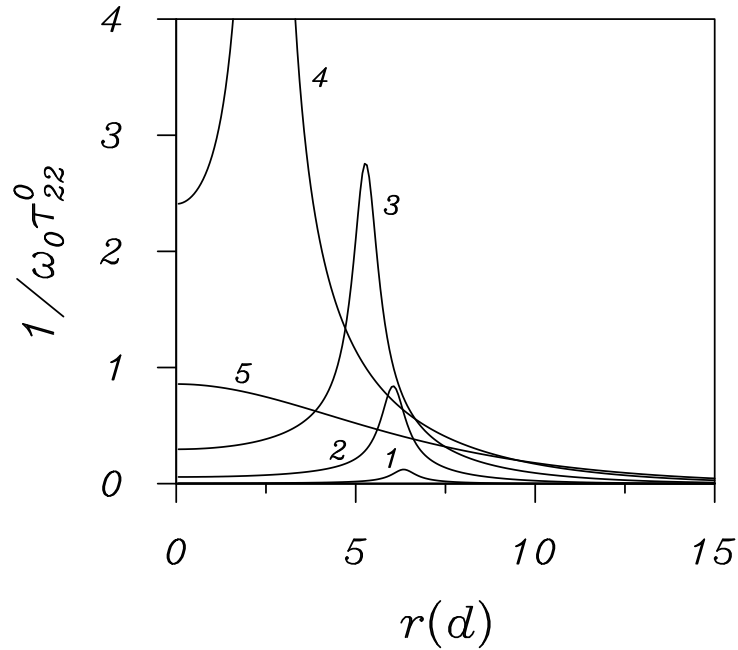


FIG. 2. The equilibrium local  $C_{22}$  collision rate  $1/\tau_{22}^0$  plotted as  $1/\tau_{12}^0$  in Fig. 1. The curves labelled 1 through 5 correspond to temperatures between 100 nK and 500 nK in steps of 100 nK.

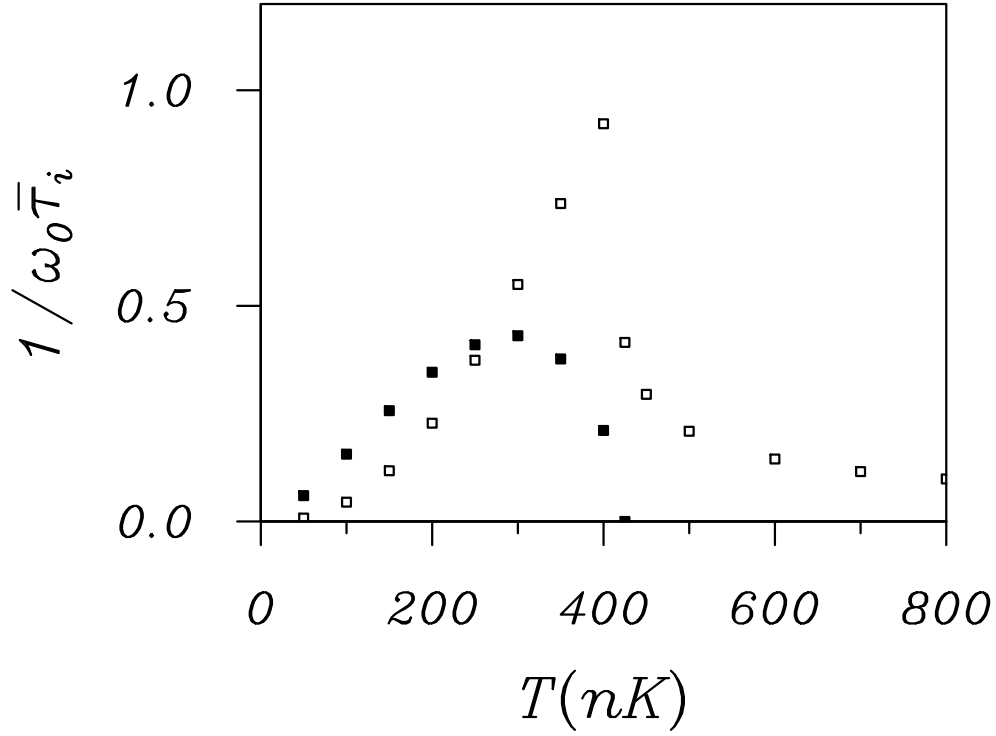


FIG. 3. Average collision rates per atom in units of the trap frequency,  $\omega_0$ , as a function of temperature. The solid squares are for  $C_{12}$  collisions and the open squares are for  $C_{22}$  collisions. The trap parameters are the same as in Fig. 1.

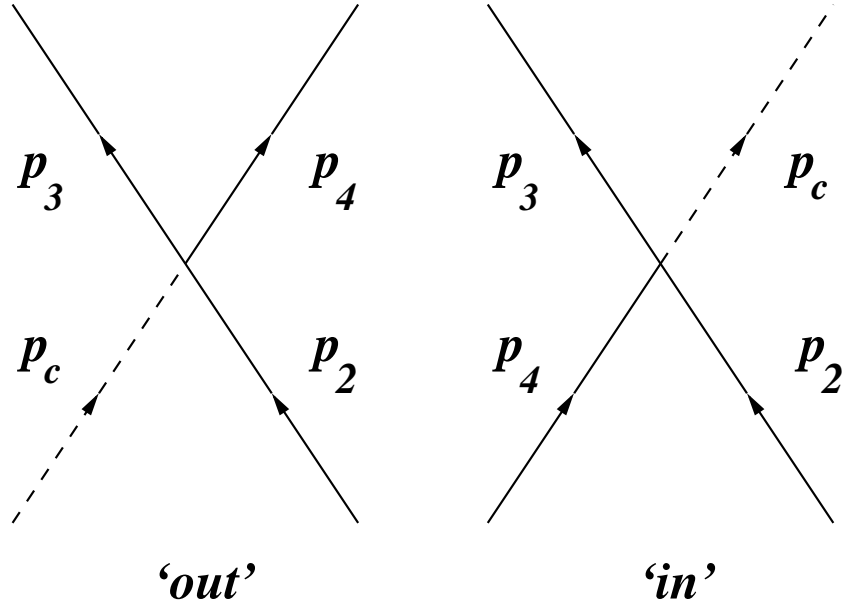


FIG. 4. Schematic illustration of the  $C_{12}$  'in' and 'out' collision processes. The dashed line represents a condensate atom and the solid lines represent thermal atoms.

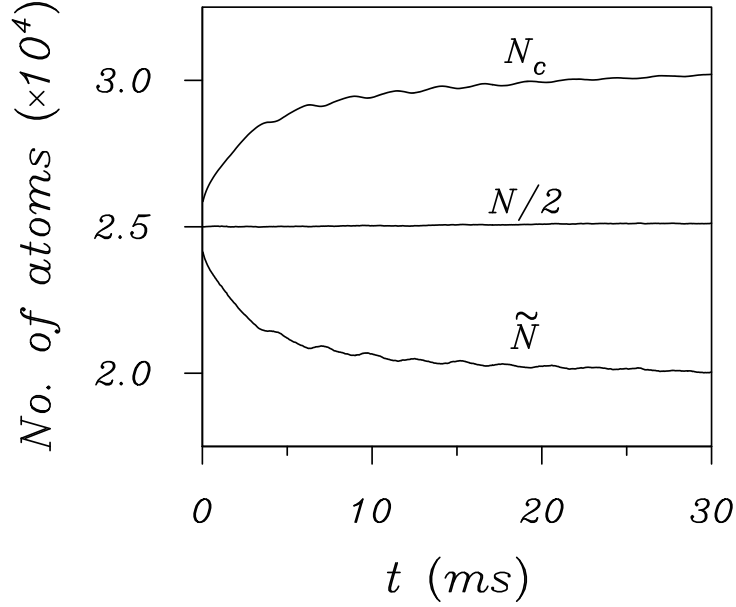


FIG. 5. The condensate ( $N_c$ ), noncondensate ( $\tilde{N}$ ) and total ( $N$ ) number of atoms as a function of time following a momentum quench. The trap has a frequency of  $\nu_0 = 187$  Hz, and contains  $5 \times 10^4$   $^{87}\text{Rb}$  atoms at an initial temperature of  $T_0 = 200$  nK.

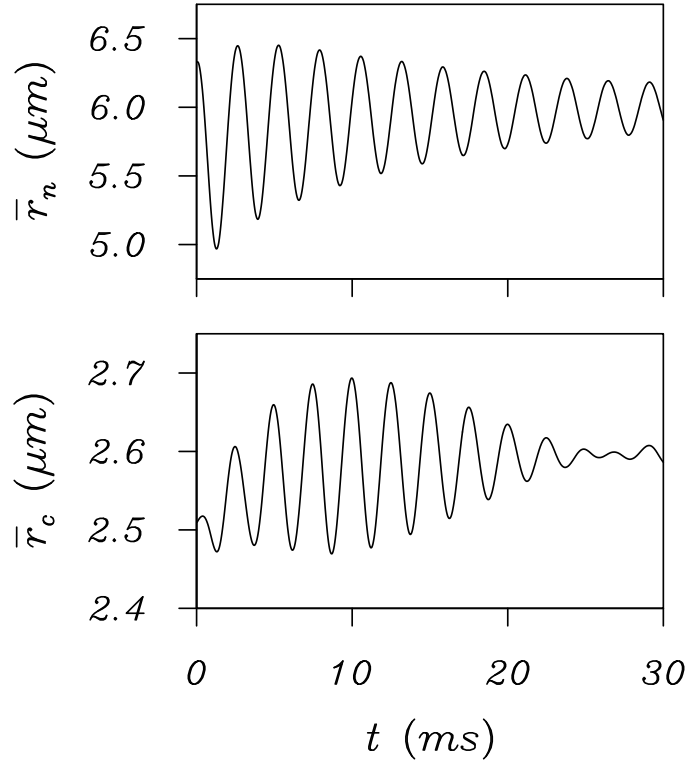


FIG. 6. The rms radius,  $\bar{r} = \sqrt{\langle r^2 \rangle}$ , as a function of time following a momentum quench;  $\bar{r}_n$  is for the thermal cloud and  $\bar{r}_c$  for the condensate.

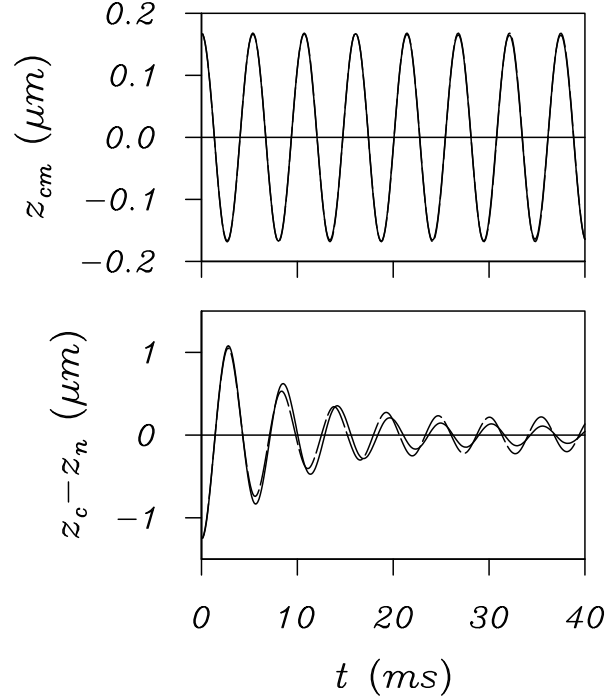


FIG. 7. The center of mass position,  $z_{cm}$ , and the displacement between the mean condensate and noncondensate positions,  $z_c - z_n$ , as a function of time. The initial conditions are given in the text. The dashed curves are in the absence of collisions, while the solid curves include both  $C_{12}$  and  $C_{22}$  collisions.

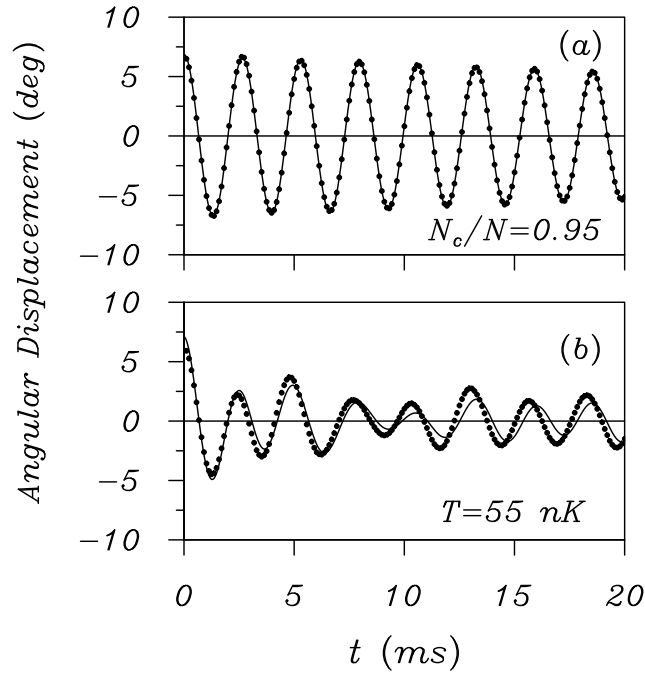


FIG. 8. Angular displacements of the condensate (a) and thermal cloud (b) as a function of time. The points are the results of the simulation and the solid lines are three-mode fits to the data. The results are for the trap studied experimentally in Ref. [23].

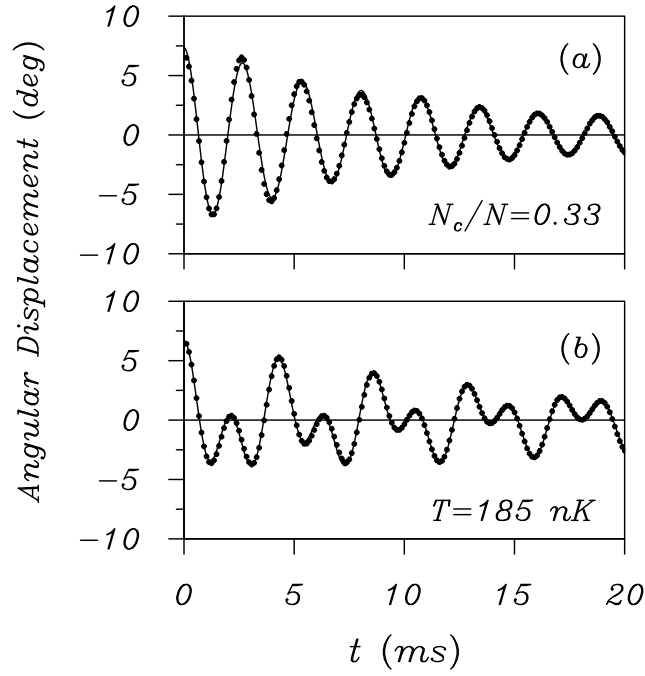


FIG. 9. As in Fig. 8 but for  $T = 185$  nK.

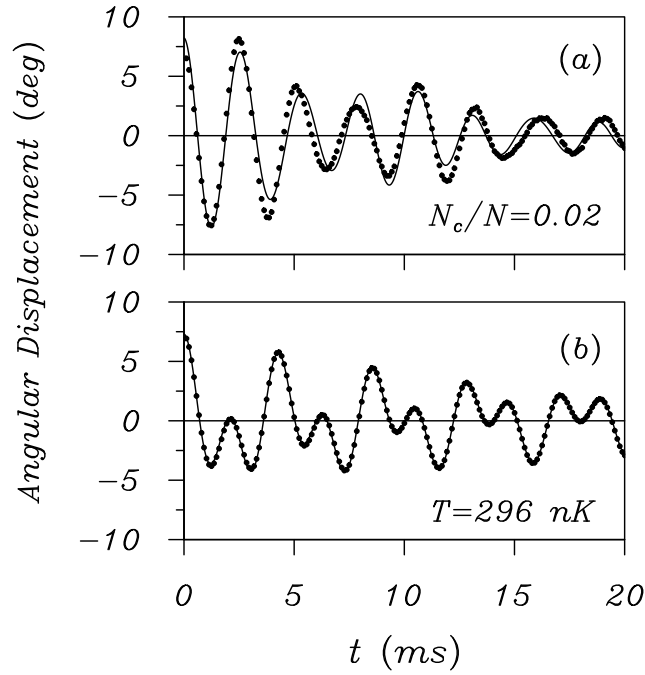


FIG. 10. As in Fig. 8 but for  $T = 296$  nK.

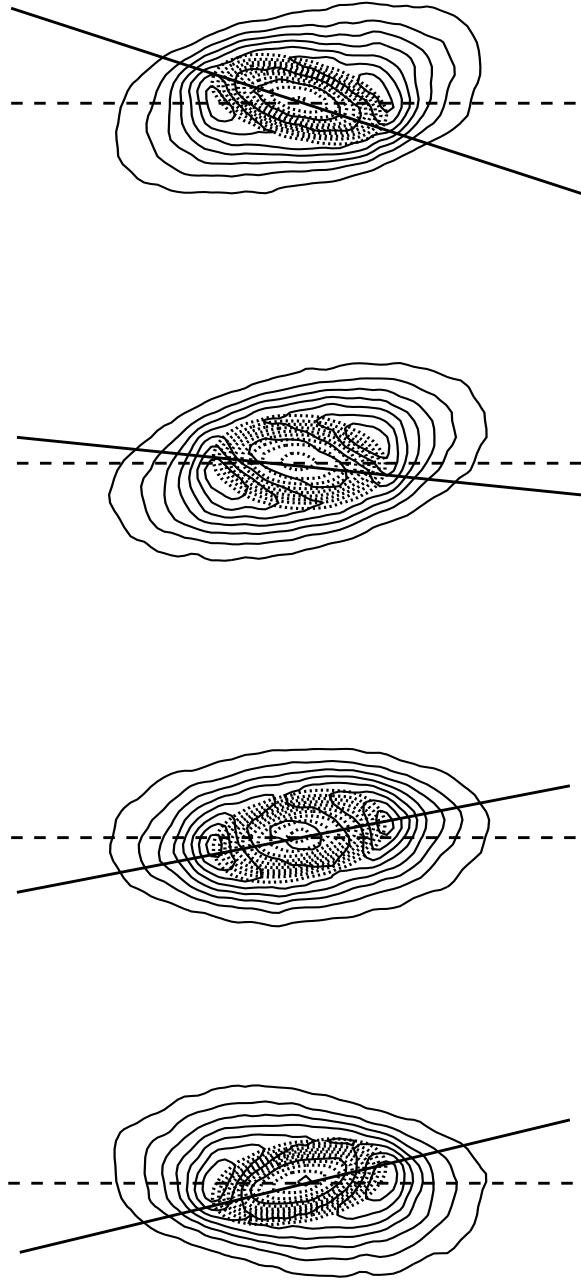


FIG. 11. Density contour plots of the condensate (dotted lines) and thermal cloud (solid lines) for a sequence of equally spaced time intervals spanning approximately one-half period of the scissors mode oscillation. The earliest time is at the top of the figure. The dashed horizontal line denotes the symmetry axis of the trapping potential and the straight solid line indicates the major axis of the condensate at each time step.

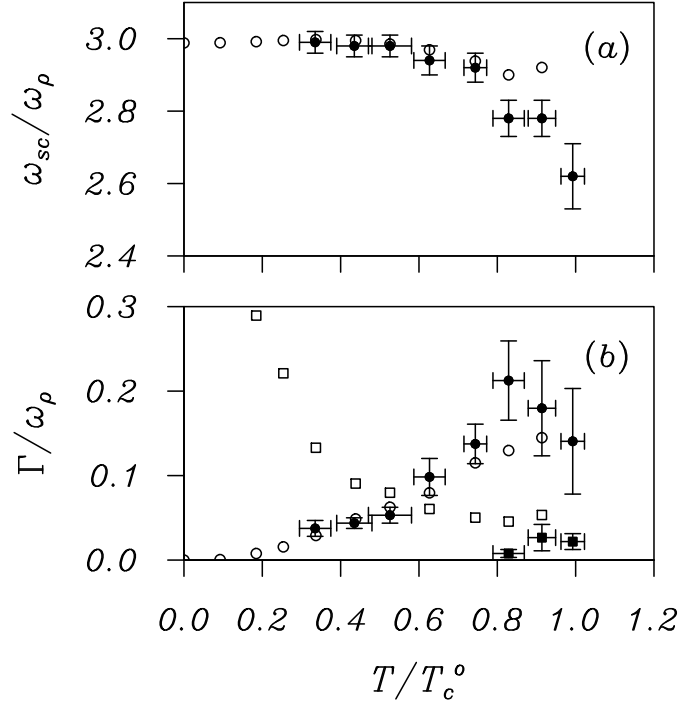


FIG. 12. Frequency (a) and damping rate (b) of the scissors modes for a variable total number of atoms, intended to simulate the experiments in Ref. [23]. The condensate mode is indicated by open (theory) and solid (experiment) circles. The open squares in (b) show the calculated average damping rate of the two thermal cloud modes, while the solid squares are the corresponding experimental values.

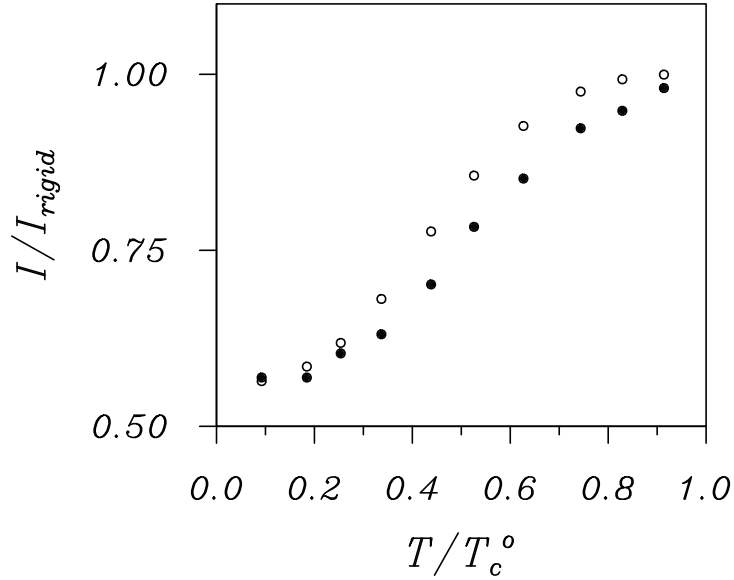


FIG. 13. The ratio of the moment of inertia of the trapped gas to the rigid body moment of inertia as a function of temperature. The solid circles are the result of Eq. (30) while the open circles are obtained using Eq. (33).